Research article

X-RAY SPECTROMETRY

Received: 29 March 2016 Revised: 17 June 2016 Accepted: 23 June 2016 Published online in Wiley Online Library: 21 July 2016

(wileyonlinelibrary.com) DOI 10.1002/xrs.2704

Focus on sulfur count rates along marine sediment cores acquired by XRF Core Scanner

S. Chéron,* J. Etoubleau, G. Bayon, S. Garziglia and A. Boissier

The aim of this study is to investigate the information provided by sulfur count rates obtained by X-ray fluorescence core scanner (XRF-CS) along sedimentary records. The analysis of two marine sediment cores from the Niger Delta margin shows that XRF-CS sulfur count rates obtained at the surface of split core sections with XRF-CS correlate with both direct quantitative pyrite concentrations, as inferred from X-ray powder diffraction (XRD) and sulfur determination by wavelength dispersive X-ray fluorescence (WD-XRF) spectrometry, and total dissolved sulfide (TDS) contents in the sediment pore water. These findings demonstrate the potential of XRF-CS for providing continuous profiles of pyrite distribution along split sections of sediment cores. The potential of XRF-CS to detect TDS pore water enrichments in marine sediment records, even a long time after sediment recovery, will be further discussed. Copyright © 2016 The Authors. X-Ray Spectrometry Published by John Wiley & Sons Ltd.

Introduction

X-ray fluorescence core scanner (XRF-CS) allows the rapid, non-destructive and semi-quantitative determination of high-resolution geochemical profiles for major, minor and a few trace elements along split wet sections of marine and lake sediment cores.[1,2] The obtained measurements are usually expressed as element count rates or ratios that can provide information about core lithology and be used in the context of palaeoclimatic applications. For example, in marine sedimentary records, down-core profiles for calcium are typically used to reconstruct the variability of biogenic carbonate accumulation related to past climate change, while Fe/Ca or Ti/Ca ratios can be taken as representative of the relative contribution of terrigenous *versus* marine sediment inputs. Down-core profiles for zirconium and bromine can also be used as proxies for grain-size and the distribution of marine organic matter in sediment cores, respectively. Many other applications have also been reported previously for sedimentological investigations.[3–6] For every measured element, the accuracy of XRF-CS analysis depends on the homogeneity, texture and smoothness of the core surface, its water content, but also on spectral resolution, counting statistic, matrix effects and effective penetration depth of analysis.[7] The most accurate results are typically obtained for elements heavier than potassium (i.e. $N > 19$). The analysis of lighter major elements such as aluminum and silicon can be severely affected by surface effects, and their determination is hence only semi-quantitative, which must be used with caution. In comparison, XRF-CS sulfur data have been rarely reported in previous studies, because of a poor XRF-CS detection efficiency and low elemental abundance and hence leading to count rates associated with a large counting statistic error.

However, in marine sediments, sulfur is typically hosted by sulfate (e.g. gypsum, anhydrite) and/or sulfide mineral phases (e.g. pyrite, marcasite), accounting to concentrations in bulk sediments of up to a few thousand ppm.[8] Substantial amounts of sulfur can also occur in the pore water, as dissolved sulfate and sulfide forms, reaching concentration levels up to about 1000 ppm.[9] Therefore, sulfur count rates measured by XRF-CS on split sections of sediment cores, which correspond to the semi-quantitative determination of total sulfur (total-S) abundances, have the potential for providing information on both solid and dissolved sulfur contents in sediment. The present study aims at investigating this possibility and assessing the parameters controlling XRF-CS total-S profiles. To this end, we analyzed two sediment cores collected at the Niger Delta continental margin, an area where intense sulfate reduction processes occur in near-surface sediment[10–13]

Materials and methods

Marine sediment cores

Two sediment cores from the Niger Delta continental margin were selected for this study. These cores were collected as part of the Guineco-Mebo (IFREMER-MARUM-University of Bremen) and ERIG-3D (IFREMER-TOTAL) scientific cruises. The Niger Delta continental margin is the location of active fluid seepage and gas hydrate occurrence in the sediment.[10–13] In such settings, the circulation of methane-rich fluids in the sedimentary column is typically associated with intense degradation of organic matter in sub-surface sediments and/or the presence of deeply buried hydrocarbon reservoirs.[14] At seepage sites, a series of geochemical and microbial processes generally lead to both dissolved oxygen and sulfate consumption near the seafloor, and, as a consequence, to the release of dissolved sulfide in pore waters and precipitation of authigenic mineral phases (including sulfides and sulfates) in the sediment.[15–18] Background information and photographs of the two studied cores are given in Table 1 and Figs 1 and 2. Core ER-CS04 was collected at the center of an active pockmark (i.e. a seafloor depression formed by fluid seepage). Note that only the top

* Correspondence to: Sandrine Chéron, Unité Géosciences Marines, IFREMER, Centre de Brest, 29280 Plouzané, France. E-mail: Sandrine.Cheron@ifremer.fr

Unité Géosciences Marines, IFREMER, Centre de Brest, 29280, Plouzané, France

Table 1. Background information of core GM-CS05 and ER-CS04

	GM-CS05	ER-CS04
Length [m]	22.38	10.61
Number of sections	23	13
Description	0–22.38 m: Homogeneous dark silty clay	0–5 m: Homogeneous dark silty clay (3.07–3.18 and 4.0–4.07 m: Homogeneous dark silty clay with carbonate concretions)
	By analogy with the study by Zabel *et al.* (2001)[28] the relatively low carbonate content indicate that sediments are dominated by terrigenous material	5–10.61 m: Dark silty clay hosting gas hydrate nodules and affected by fissures and cracks ascribed to gas exsolution and expansion

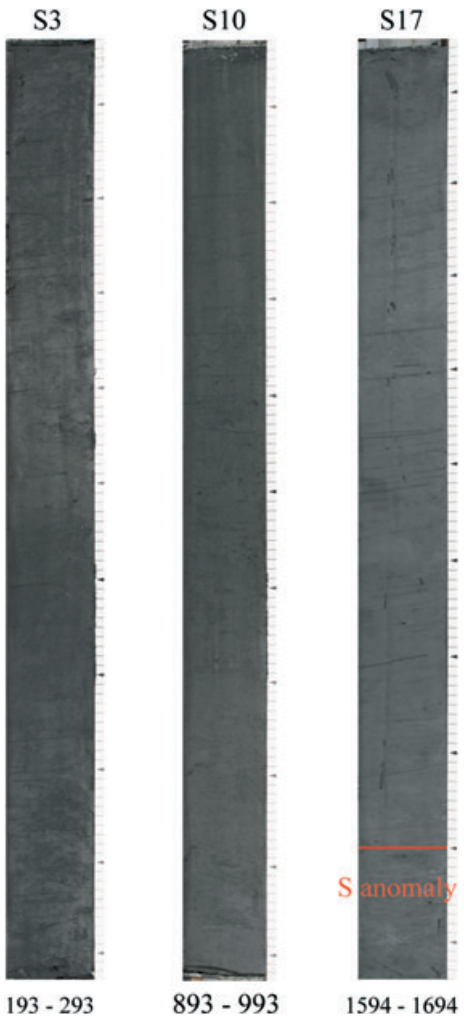

Figure 1. Pictures of three split sections of core GM-CS05: Section 1 is rich in Ca while section 10 is rather depleted and section 17 presents the anomaly of sulfur (orange marker). Note that no significant difference can be visually observed between the different sections.

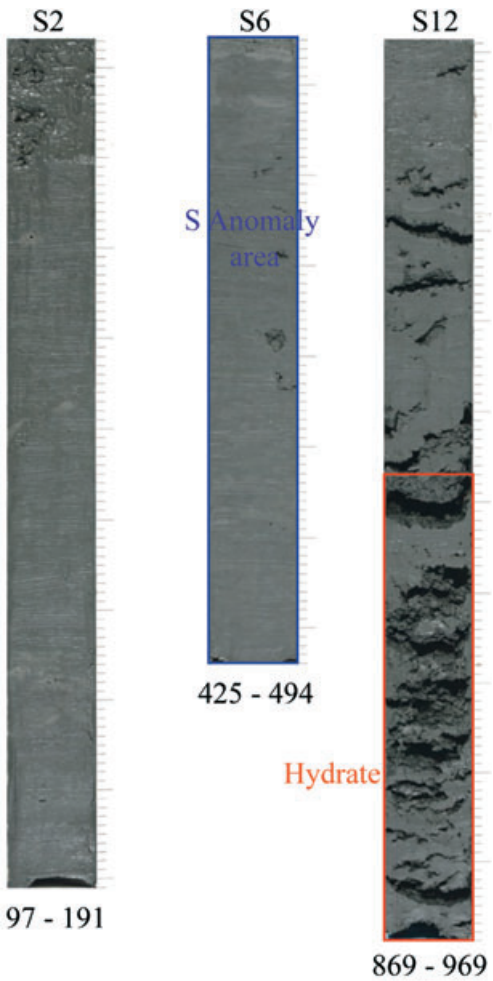

Figure 2. Pictures of three split sections of core ER-CS04: No anomaly has been detected in section 2 while a high sulfur anomaly was measured in section 6. Section 12 shows the fissures and cracks associated with the dissociation of gas hydrates after core recovery.

5 m of core ER-CS04 was analyzed by XRF-CS because the bottom part of the core (from 5-m to 9-m depth) was heavily disturbed because of the presence of massive gas hydrates and free gas in the sediment. Core GM-CS05 was recovered at a site considered as a reference site located at the outside periphery of another pockmark. After core recovery, 1-m-long sections were split in two halves to carry out XRF-CS and pore water geochemical measurements onboard.

For core GM-CS05, sediment samples were systematically collected every 10 cm along the split core for X-ray powder diffraction (XRD) and wavelength dispersive X-ray fluorescence (WD-XRF) analyses. Additional samples were collected at intervals corresponding to enhanced XRF-CS total-S count rates. Wet samples were placed into an oven at 60 °C for 48 h. Then about 20 g of dried sediment was crushed in an agate mortar. Overall, about two hundred

samples were analyzed by XRD, and almost thirty samples were processed for combined XRD and WD-XRF quantitative determinations. For core ER-CS04, 23 sediment samples were taken between 0-cm and 911-cm depth below the seafloor (bsf). These samples were dried, crushed (according the same protocol described for core GM-CS05) and analyzed by WD-XRF. In parallel, 11 pore water samples were collected and analyzed onboard to determine total dissolved sulfides (TDS) and dissolved sulfates.

X-ray fluorescence

The XRF-CS used in this study is manufactured by ***AVAATECH*** and mounted in a 20-feet sea container. The system is based on energy-dispersive XRF (ED-XRF) using an ***OXFORD*** Rh X-ray anode tube 50 W, a ***CANBERRA*** Silicon Drift Detector (SDD) cooled thermoelectrically (energy resolution of 150 eV at 5.9 keV) and five interchangeable filters. Prior to analysis, the surface of the wet sediment core section was carefully flattened with a spatula, and covered with a thin Ultralene® foil (4 μm thick) to prevent any contamination, oxidation and drying. The depth of surface sediment analyzed by XRF-CS generally does not exceed a few tens of microns. A thin water film typically forms at the interface between the sediment surface and the Ultralene® foil, which decreases elemental count rates by absorption. The size of the sediment area irradiated corresponds to a rectangle of 10 mm length × 16 mm width. The step of analysis was set up to 10 mm in order to acquire a continuous record of elemental compositions along the sediment cores. The portions of the cores exhibiting cracks, holes or any disturbed sediment were systematically discarded for the analysis. The measurement time was 10 s for each individual step analysis. For light elements, from Al to Fe (including S), the operating analytical conditions were set up to 10 kV and 600 μA, without primary filter. The measurements were performed under helium medium. For heavy elements, from Fe to Mo, the operating analytical conditions were set up to 30 kV and 1000 μA, with Pd-Thick as primary filter. Finally, Ba count rates were determined at 50 kV and 1000 μA with Ag as primary filter. Each spectrum deconvolution of K and L analytical lines was done with the WinAxil software package, which provides for any element an individual peak area converted in counts. To a first approximation, the count rates are proportional to corresponding elemental concentrations in the sediment. Characteristic S emission Kα line is 2.3 keV close to L lines Rh anode tube. It is relatively free of spectral interferences and the main absorber elements are phosphorous and silicon which have a negligible influence on S measurements.[20]

Quantitative determination of total-S concentrations in selected sediment samples was obtained by fully automated WD-XRF equipment (***BRUKER*** S8 Tiger), i.e. a sequential X-ray spectrometer using an end window Rh anode tube. Quantitative elemental total-S and sulfate-bearing sulfur (sulfate-bearing S) concentrations were performed from the S Kα line under vacuum with a voltage of 30 kV and an intensity of 135 mA, using a crystal Ge, a collimator 0.46° and a flow counter for detection. Time measurement was 60 s on sample in rotation (60 rpm/mn). Samples were prepared as fused beads, using two separate fusion methods for WD-XRF analysis. For sulfate-bearing S determination, the fusion bead sediment powder sample was pre-ignited at 1050 °C to volatilize unstable forms of sulfur. One aliquot of 0.5 g of calcined powder was fused with 9 g of Spectroflux 120A ($Li_2B_4O_7$ 90% – LiF 10%, ***Johnson Matthey***), 500 μl of a 250 g/l solution of LiBr (***ACROS***) as no-wetting agent was added. The fusion was performed in a Pt–Au crucible at 1050 °C placed in a muffle furnace under air. This preparation also serves for measuring the other major element concentrations. For total-S determination, 0.2-g dried samples (110 °C) were first oxidized gradually during 1 h, from ambient temperature to 500 °C, in the presence of an oxidizing agent ($LiNO_3$) to prevent losses of sulfide or elemental sulfur during the fusion (1000 °C). We introduced successively 6 g of Spectroflux 161 ($Li_2B_4O_7$ 90% – $LiNO_3$ 10%, ***Johnson Matthey***), 0.2 g of sample dried at 110 °C at the center without any contact with the inner surface of the Au–Pt crucible, 0.3 g of no wetting agent NaBr (***MERCK***) and then carefully recovered with another 2 g of Spectroflux 161 and 3 g of Spectroflux 106 ($Li_2B_4O_7$ 85% – La_2O_3 15%, ***Johnson Matthey***). Calibrations were established using a set of certified materials obtained mainly from the ***Canadian Certified reference materials*** Project (CCRMP): UM-1, UM-2, UM-4, WMG-1, ***Geological Survey of Japan*** (GSJ): JB-3, JCFA-1, JLs-1, JSD-2 and the ***Centre de Recherches Pétrochimiques et Géochimiques in France*** (CRPG):BE-N, IF-G and by doping an in-house standard with 'zero' sulfur concentration with increasing amounts of a 10 000 ppm sulfur plasma solution (***Alfa Aesar***) in the 0 to 50 000-ppm calibration range concentration. The large dilution of the sample in the flux in the two preparations avoids matrix effects and provides homogeneous glass-disks. Characteristic S line net intensities were correlated with certified concentrations to determine linear calibration curves. The precision is reported here as relative standard deviations[21] (RSD), which correspond to 2.5% ($n = 9$) and 3.8% ($n = 17$) for sulfate-bearing S and total-S determinations, respectively. The detection limits (DLs) were estimated to be better than 500 ppm for both preparations.

WD-XRF quantitative analyses can be used to calibrate the elemental profiles obtained by XRF-CS. However, because of errors inherent to the presence of a thin surficial water film, to variations in particle size along the core, or to any other effect that could potentially influence XRF-CS measurements, a simple linear regression between quantitative WD-XRF analyses and XRD-CS count rates cannot be applied. Instead, we decided to implement the log-ratio calibration method described previously by Weltje and Tjallingii (2008)[19] and Weltje *et al.* (2015).[22] This can be done using the AvaaXelerate software package developed by Menno Bloemsma.[23]

X-ray diffraction

The presence of pyrite in selected sediment samples was determined by X-ray diffractometry (XRD), using a D8 Advance ***BRUKER*** model, a device type Bragg–Brentano equipped with a Cu X-ray tube, a primary Soller slit of 0.6 mm, a nine-position sample holder and the ***VANTEC-1*** Position Sensitive Detector with a nickel filter (Ni 0.5). Prior to analysis, dried sediment powders were inserted into the sample holder, and flattened. Measurements were made from 5 to 70° with a step of analysis of 0.01° lasting 1 s. The voltage and amperage were set up to 40 kV and 30 mA, respectively. Qualitative analysis of the diffraction pattern of unknown sample was carried out using the identification phase procedure of the software. The pyrite Bragg reflections and Intensity (I/Io) occur at 1.6332 (1), 2.709 (0.85) and 2.423 (0.65) Angstroms. Quantitative analyses were performed according to the Rietveld refinement method[24–26] using the ***BRUKER*** program ***TOPAS***. This method is based on a least squares approach to refine a theoretical line profile until it matches the measured profile. It assumes that all mineral phases present in the mixture have been identified and that the sum of all phase quantities is 100%. Pyrite amount can be measured at low abundance, given that the DL experimentally determined on

a pure clay sample corresponds to a concentration of 0.5% and the precision on the repeatability of measurement is 6% ($n = 10$).

Pore water measurements

Upon core recovery, pore water samples were immediately collected at selected sediment depth for geochemical analyses. Concentrations for TDS and dissolved sulfates were determined on-board immediately after sampling by colorimetry (***Spectro Libra S11***) and ion-chromatography (***DX120 Dionex***),[12] respectively.

Experimental procedures

As mentioned above, a film of water typically forms under the thin Ultralene® foil that covers the sediment core.[27] In this study, we conducted a series of experiments to investigate the extent to which the presence of dissolved sulfur in pore waters (from both sulfates and/or sulfides) may control some of the total-S signal measured by XRF-CS in marine sediment cores. To do so, aliquots of dried sediment powder (5 g) were thoroughly mixed with 20 ml of increasing amounts of dissolved S in a saline solution (35 g/l pure NaCl ***Merck*** in mQ water). Dissolved S solutions were prepared in the range of 0 to 2000-ppm concentrations by appropriate dilution of 10 000-ppm sulfur ICP standard (***Johnson Matthey***) mother solution in mQ water. The mixtures were then centrifuged for 15mn (3000 rpm) and the supernatant discarded. The moisture of each individual wet sediment preparation was checked to be about 50%. Then, the impregnated wet sediments were placed into a sample holder consisting of a plastic bar drilled with cells of 33-mm diameter and 3-mm depth at regular intervals, flattened and covered with the Ultralene® foil. The measurements were performed with the same analytical parameters as for the core section analysis.

Results and discussion

As mentioned above, sediment core total-S profiles acquired by XRF-CS are generally not reported in scientific papers because the XRF-CS detection efficiency is low and abundance variations weak, hence providing a poor count rate N with a large counting statistic error. Sulfur determination is part of simultaneous detection of neighbour light elements present in seawater and sedimentary matrix. In the following study, we present two cases where the total-S profiles obtained by XRF-CS display distinctive enrichments.

Core GM-CS05

Core GM-CS05 displays an almost flat total-S raw profile punctuated by distinct pronounced enrichments (e.g. 1680-cm depth; Fig. 3). When comparing the different elemental raw profiles obtained for that core, one can note that the Fe downcore profile is anti-correlated with that for Ca, a consequence of the relative dilution of the Fe-rich terrigenous signal (hosted mostly by detrital clays) by changing proportions of carbonates downcore, and vice versa. There are however a few exceptions to this general trend, which

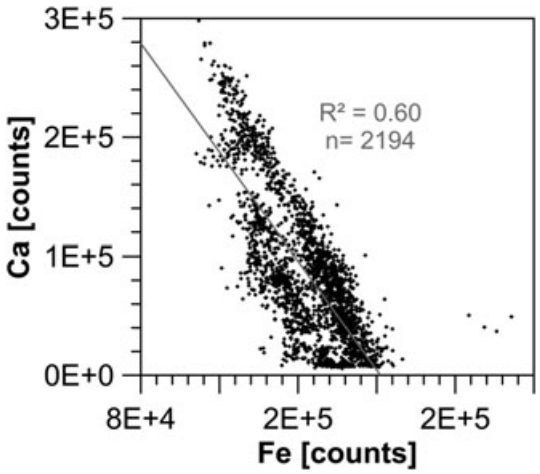

Figure 4. Core GM-CS05. Anti-correlation between the Fe profile measured by XRF-CS and Ca profile measured by XRF-CS.

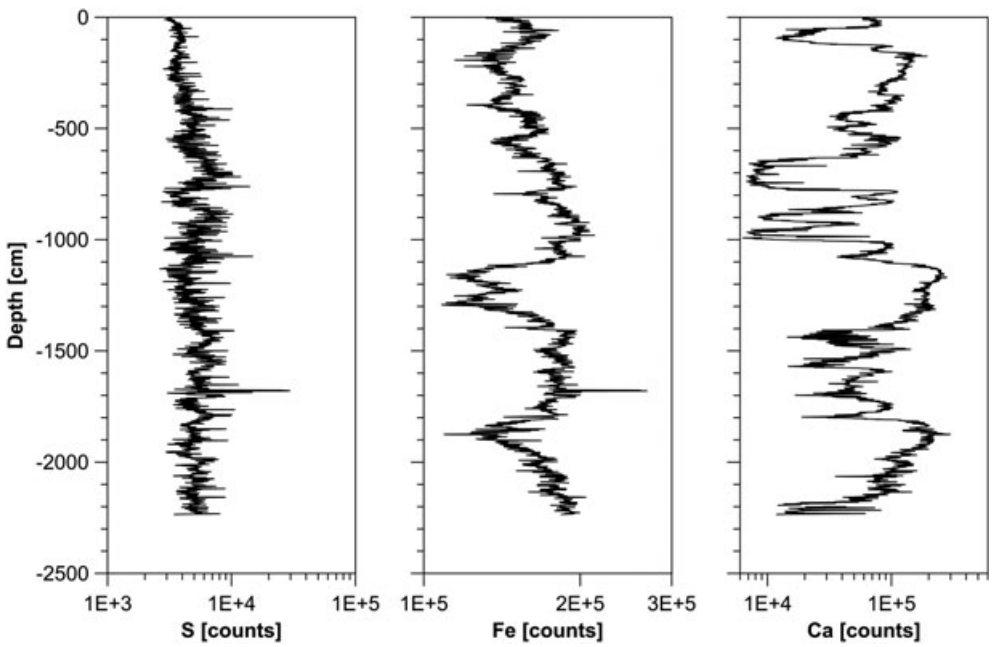

Figure 3. Core GM-CS05. Total-S raw profile, Ca raw profile and Fe raw profile measured by XRF-CS *versus* depth.

concern a few points characterized by particularly high XRF-CS count rates for Fe (around 250 000cts) (Figs 3 and 4). Evidence that these Fe-rich points are also associated with high total-S count rates suggests that sulfur enrichments in core GM-CS05 could be controlled by the presence of Fe-sulfide phases within the sediment.[1] To test this hypothesis, precise quantifications of both total-S and sulfate-bearing S concentrations were performed by WD-XRF on about 30 discrete samples collected along core GM-CS05 (see protocol described above). These quantitative data are reported in Table 2. Total-S concentrations vary from 0.38% to 5.78% downcore, while sulfate-bearing S varies from 0.10% to 0.92%.

At first, when plotted *versus* sediment depth (Fig. 5), the high resolution total-S profile obtained by XRF-CS agrees very well with the total-S determined quantitatively by WD-XRF. In particular, we observe the same sulfur anomaly at around 1680-cm depth, which provides evidence that this latter does not correspond to any surficial enrichment or to an analytical artefact. In contrast, the XRF-CS total-S profile exhibits no particular correlation with sulfate-bearing S concentrations (Fig. 5). The above observations clearly suggest that the downcore XRF-CS total-S signal is controlled primarily by the presence of sulfide phases within the sediment. Note that these concentrations are above DL of WD-XRF previously given. Using the concentrations of total-S and sulfate-bearing S determined by WD-XRF, we can calculate estimates for pyrite concentrations in the sediment, yielding values ranging from 0.28 to 9.58% (m/m).

Second, we also calibrated the total-S profiles obtained by XRF-CS with the AvaaXelerate software package, using calcium as the denominator (see Section 1b). The obtained high resolution calibrated total-S profile is expressed in relative concentrations (Fig. 6).

Table 2. Core GM-CS05. Quantitative analysis (m/m) of major elements such as total-S and sulfate-bearing S by WD-XRF, and estimate of pyrite by WD-XRF

Depth	SiO_2	Al_2O_3	Fe_2O_3	CaO	MgO	K_2O	TiO_2	P_2O_5	LOI (1050 °C)	S-sulfate	Total	S total	Pyrite estimated
cm	%	%	%	%	%	%	%	%	%	%	%	%	%
19	40.76	18.40	7.52	6.94	2.02	1.67	0.82	0.14	18.10	0.22	100.15	0.38	0.28
118	43.17	21.07	7.45	3.49	2.04	1.69	0.84	0.11	16.67	0.13	100.19	0.54	0.75
219	36.21	15.83	6.07	12.8	2.06	1.17	0.76	0.14	21.67	0.29	100.13	0.41	0.21
329	39.65	18.13	7.02	8.39	2.05	1.57	0.77	0.11	17.64	0.58	100.09	0.85	0.49
409	39.41	17.28	6.85	9.24	2.07	1.53	0.73	0.11	18.36	0.65	100.59	1.16	0.94
503	43.91	20.54	7.66	3.51	2.09	1.68	0.76	0.09	16.79	0.13	100.32	1.08	1.77
503	43.60	20.58	7.55	3.39	2.09	1.65	0.75	0.10	16.65	0.21	99.808	1.08	1.62
583	40.69	17.53	6.76	8.33	2.32	1.72	0.82	0.12	18.00	0.21	99.729	0.58	0.68
642	46.35	21.47	8.19	1.20	2.26	1.76	0.75	0.10	14.58	0.16	100.18	1.12	1.78
672	46.92	21.47	8.29	0.78	2.26	1.87	0.74	0.10	14.15	0.18	100.17	1.33	2.15
714	47.25	22.19	8.18	0.78	2.23	1.93	0.76	0.10	13.55	0.16	100.34	1.29	2.11
716	46.65	21.84	8.28	0.74	2.17	1.88	0.75	0.10	14.68	0.15	100.41	1.22	1.99
718	46.77	22.05	8.05	0.69	2.17	1.88	0.75	0.10	14.48	0.15	100.20	1.27	2.09
760	46.63	22.23	7.98	0.89	2.14	1.87	0.83	0.10	14.29	0.10	100.02	0.98	1.63
762	46.72	22.33	8.22	0.99	2.18	1.86	0.85	0.11	14.12	0.13	100.55	1.01	1.63
789	39.97	18.55	6.94	8.21	2.21	1.70	0.82	0.12	18.62	0.13	100.21	0.48	0.65
869	44.25	21.60	8.56	2.25	2.11	1.75	0.77	0.10	15.85	0.12	100.35	1.49	2.55
879	42.17	20.20	9.19	4.36	2.04	1.71	0.74	0.10	15.73	0.38	99.95	2.00	3.50
959	47.19	22.30	8.48	0.67	2.20	2.06	0.81	0.11	13.03	0.11	99.69	1.08	1.95
1059	41.51	19.13	7.94	6.17	2.22	1.74	0.80	0.13	16.67	0.21	99.47	1.21	1.86
1072	44.91	21.10	7.84	2.92	2.26	1.90	0.82	0.11	15.22	0.09	99.915	0.92	1.54
1074	45.62	21.56	7.89	2.67	2.31	1.94	0.82	0.11	14.97	0.10	100.81	0.94	1.57
1076	45.18	21.16	7.72	2.81	2.27	1.97	0.82	0.11	15.26	0.10	100.19	0.93	1.55
1120	34.84	14.72	5.71	14.8	2.06	1.09	0.75	0.17	21.52	0.52	99.43	0.64	0.87
1160	30.72	12.63	5.29	20.1	1.80	0.84	0.67	0.11	23.21	0.82	99.62	0.9	1.17
1208	34.98	14.90	5.52	15.2	2.07	1.05	0.74	0.11	21.23	0.57	99.67	0.65	0.86
1349	39.53	17.81	6.92	9.51	2.15	1.68	0.83	0.10	16.14	0.86	99.44	1.11	1.53
1408	44.21	20.67	7.85	3.78	2.32	1.81	0.84	0.10	15.93	0.23	100.63	1.39	2.45
1419	45.39	21.47	7.84	2.68	2.35	1.83	0.85	0.10	15.23	0.14	100.60	1.24	2.23
1549	45.37	21.75	7.99	2.18	2.27	1.90	0.86	0.10	14.83	0.16	100.08	1.55	2.80
1559	46.42	22.22	8.45	1.73	2.34	1.97	0.83	0.10	14.30	0.20	101.40	1.88	3.39
1579	43.90	21.60	7.61	4.31	2.21	1.82	0.82	0.10	15.64	0.24	101.02	1.17	2.04
1679	41.15	20.85	12.9	2.86	1.90	1.63	0.84	0.09	15.82	0.42	101.38	5.78	10.56
1800	44.79	21.16	7.28	3.17	2.31	1.85	0.85	0.11	15.43	0.17	99.82	1.26	2.25
1869	33.59	14.61	5.86	16.1	1.95	1.07	0.70	0.11	21.75	0.92	100.37	1.23	1.73
1929	37.52	16.59	6.35	12.0	2.16	1.45	0.77	0.11	19.03	0.60	99.82	1.11	1.70
2039	42.82	19.46	7.40	5.98	2.30	1.82	0.89	0.10	15.99	0.38	100.05	1.19	1.99
2099	42.38	19.51	7.48	6.18	2.25	1.81	0.88	0.10	15.90	0.52	100.15	1.26	2.03
2179	44.86	21.16	8.33	2.55	2.29	1.94	0.94	0.11	14.52	0.24	99.70	1.83	3.27

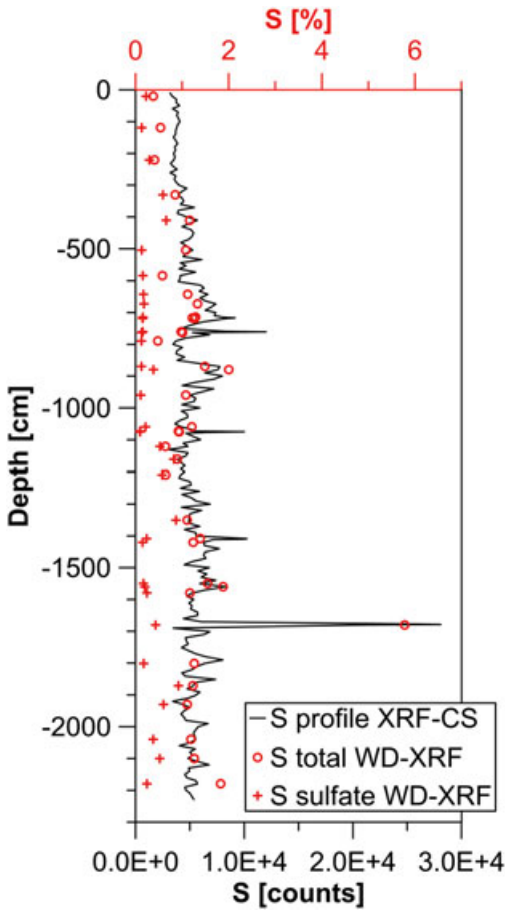

Figure 5. Core GM-CS05. High resolution (1 cm) total-S profile obtained by XRF-CS (in black) compared the quantitative total-S (red circles) and sulfate-bearing S (red cross) measured by WD-XRF in selected sediment samples.

The above-mentioned hypothesis is also further supported by mineralogical analyses obtained by XRD on the same samples, which show that pyrite (FeS_2) is the only S-bearing crystalline mineral phase in our 200 discrete sediment samples (Fig. 7). In these sediments, the main mineralogical phases are clays, micas, quartz and halite. For each mineralogical phase, the weight abundances (m/m) were determined using the Rietveld method, thus obtaining mineralogical profiles with a resolution of 10 cm (Fig. 8). The calcite and clays profiles appear to be anti-correlated. To some extent, this reflects the fact that apart from calcite and clays, other sediment-bearing mineral phases exhibit little downcore variations. For example, halite varies between 3% and 9% wt, quartz between 4% and 10% and pyrite is between <0.5% and 3.3% with a peak of 6.8%. These pyrite concentrations are similar or above the DL of quantification by XRD (0.5%). Despite these low values, the downcore evolution of pyrite abundance obtained by XRD is in good agreement with the calibrated XRF-CS total-S profile (Fig. 9), in particular for the S-rich sediment horizon at 1680 cm. However, it should be noted that an offset exists at the top of the core between profiles for XRF-CS total-S and pyrite concentrations measured by XRD, which may be because of high water content near the sediment surface. Indeed, sulfur, a light element, is expected to be more sensitive to this parameter that the calcium used as the denominator for normalization.

XRD may be a valuable tool for bulk sample mineralogical characterization and for quantifying the abundance of pyrite and other sulfide-bearing minerals in sediments. However, high-resolution investigations of pyrite distribution along sediment cores would require fastidious and time consuming sample preparation and analysis. As shown above, the good relationship observed between total-S profile obtained by XRF-CS and pyrite abundances indicates that the XRF-CS total-S signal is mainly controlled by the presence of pyrite in the sediment. As a consequence, a quick semi-quantitative determination of pyrite distribution along marine

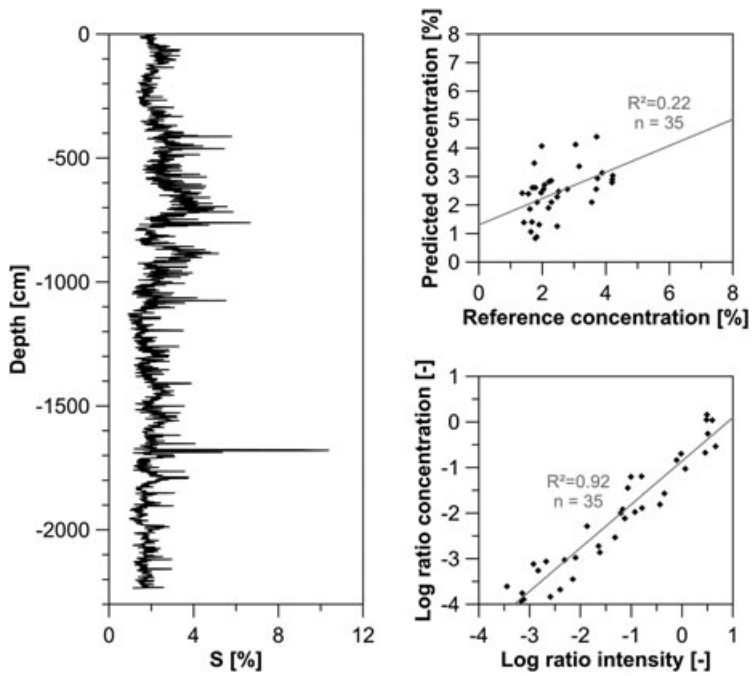

Figure 6. Core GM-CS05. High resolution total-S profile calibrated obtained by XRF-CS. This profile has been calibrated according to the equations derived from cross-plots of total-S predicted concentrations *versus* total-S reference concentrations and Log (S/Ca) intensity *versus* Log (S/Ca) concentration as presented to the right.

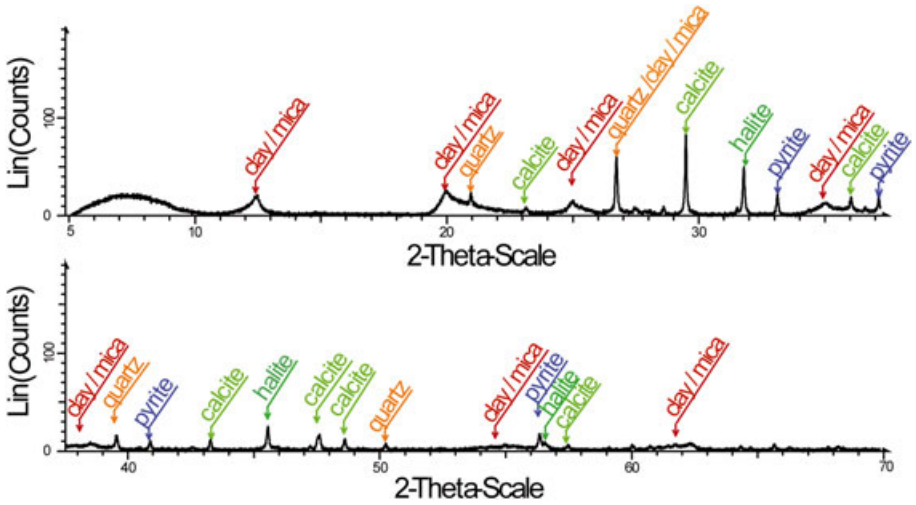

Figure 7. Core GM-CS05. Example of diffractogram obtained on a selected sediment sample.

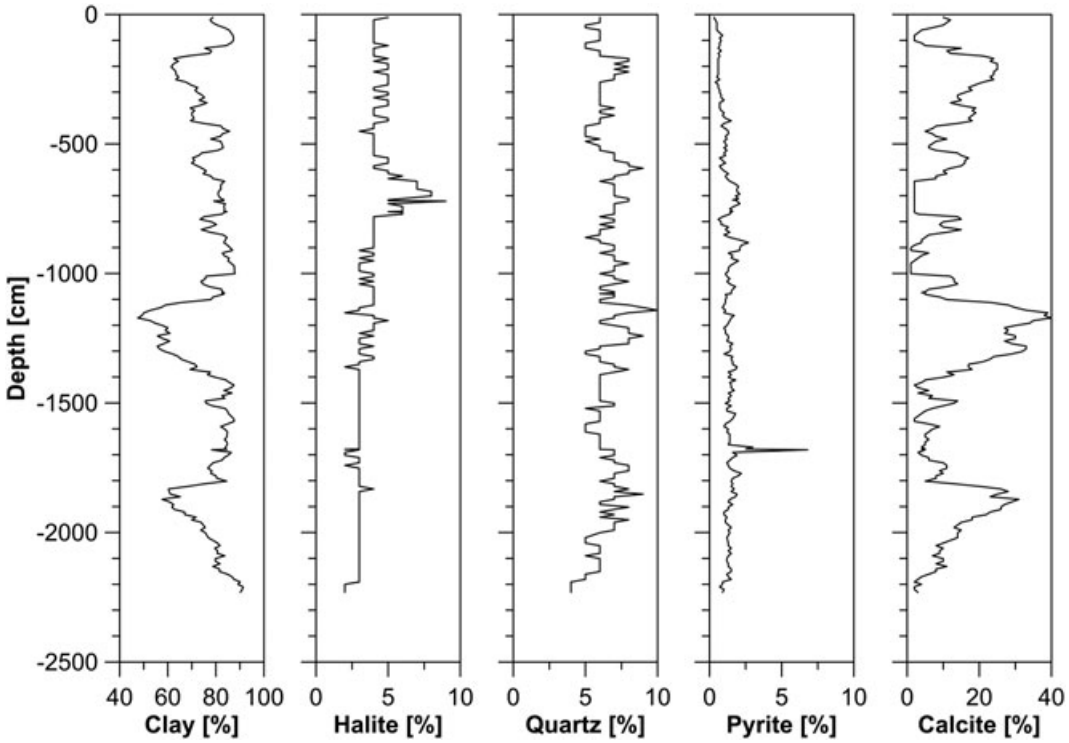

Figure 8. Core GM-CS05. XRD profile obtained from series of sample selection analysis along core.

sediment cores could be achieved using XRF-CS, under routine analytical conditions simultaneously with the measurement of other light elemental profiles, even at a low concentration. However, this analysis should be combined with a few quantitative XRD and WD-XRF measurements on a series of selected samples in order to assess the potential presence of sulfate *versus* sulfide minerals in the sediment.

Core ER-CS04

In contrast to core GM-CS05, core ER-CS04 collected at the center of a hydrate-bearing pockmark displays a pronounced sulfur enrichment between about 400-cm and 500-cm depth, while the overlying part of the core is characterized by lower total-S count rates (Fig. 10).

Interestingly, this sulfur enrichment coincides with the peak of TDS contents measured on board for corresponding pore waters (i.e. exhibiting a maximum concentration of about 225 ppm) (Fig. 10).

Several hypotheses could possibly explain the origin of this sulfur enrichment identified by XRF-CS. First, this enrichment could be related to high levels of total-S concentrations in the sediment. To test this hypothesis, we analyzed a total of 23 samples collected along the core with a resolution of about two samples per meter

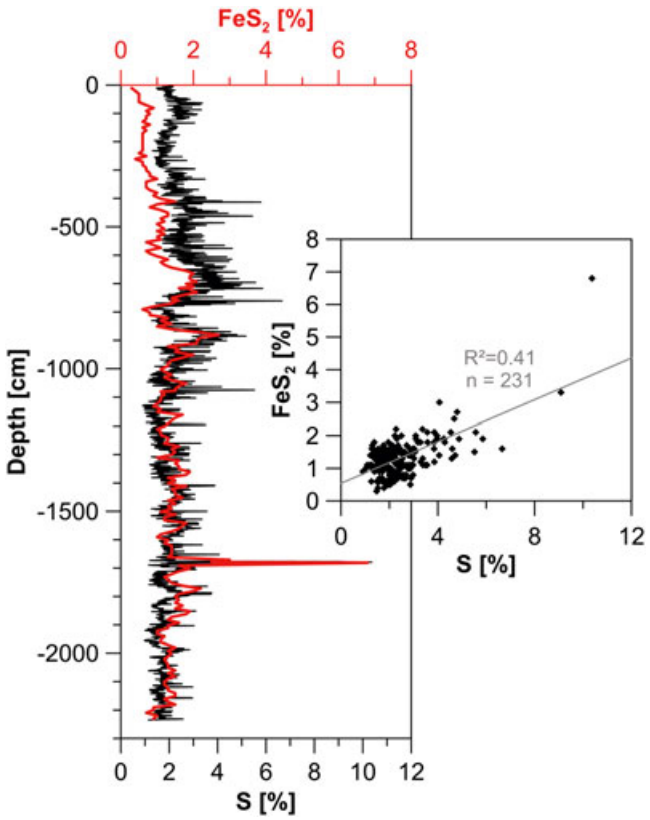

Figure 9. Core GM-CS05. XRF-CS total-S profile calibrated (in black) compared to XRD (resolution 10 cm) record for pyrite (in red) *versus* depth, in core GM-CS05. The inlet shows the calibrated S concentration *versus* the pyrite concentration.

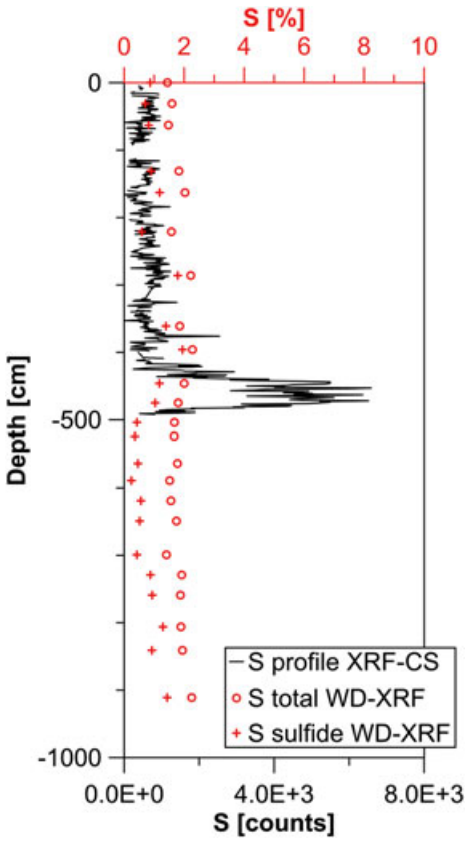

Figure 11. Core ER-CS04. High resolution total-S profile measured by XRF-CS (in black) compared with total-S (red circle) and sulfide-bearing S (red cross) in selected sediment samples measured by WD-XRF *versus* depth.

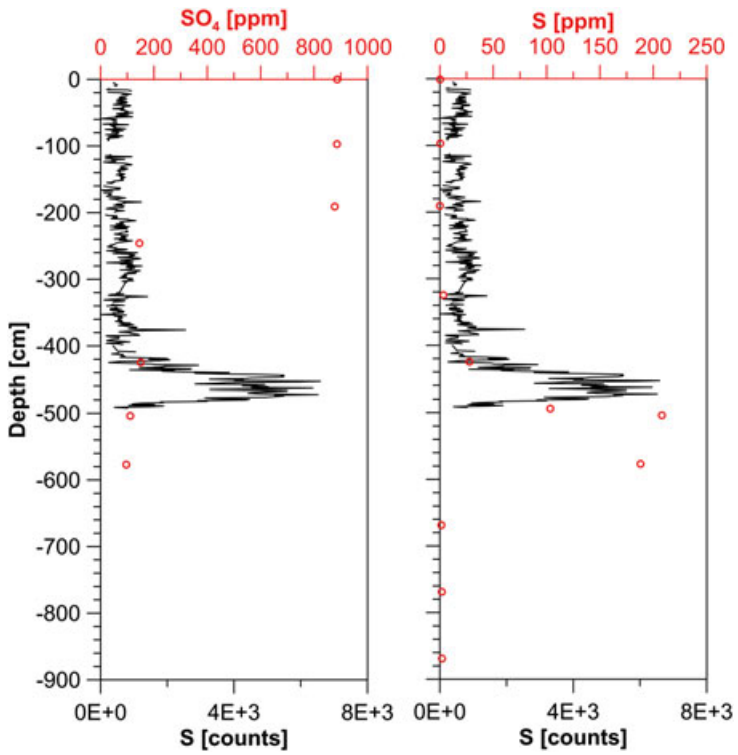

Figure 10. Core ER-CS04. High resolution (1 cm) XRF-CS total-S profile (in black) compared with dissolved sulfate (red circles) in pore water on the first graph and with total dissolved sulfide contents on second graph (red circles).

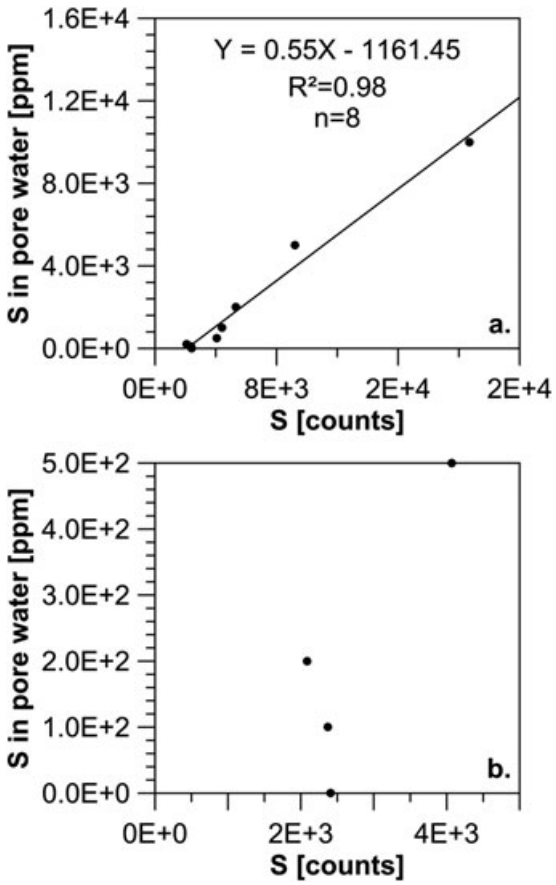

Figure 12. Core ER-CS04. Above: S XRF-CS intensities on test core and doped with S solution (cts) *versus* S concentration added to sediment to simulate the presence of sulfur in pore water (ppm) Below: close-up on the graph above showing the limit of quantification of the method.

before and after the anomaly and a higher resolution near the observed anomaly. Precise quantifications of S-total and sulfate-bearing S were performed by WD-XRF using the protocol described previously, and sulfide-bearing sulfur (sulfide-bearing S) was deduced from these measures. The total-S and inferred sulfide-bearing S concentrations range between 1.41% and 2.28% and 0.42 and 1.95%, respectively. However, the total-S obtained by WD-XRF along core ER-CS04 does not show any particular enrichment that could account for the observed sulfur enrichment contrary to the total-S profile by XRF-CS. This suggests that this anomaly is not because of the presence of sulfur in the sediment (Fig. 11).

Alternatively, the high total-S count rates could also be explained by the presence of S-rich pore waters or by a localized enrichment in solid sulfur at the surface of the split core section. To test this possibility, we performed a series of experiments, by mixing sediments with S-doped deionized water in order to reproduce interstitial water enriched in sulfur (see section 2e). These experiments showed that total-S XRF-CS intensities display a linear correlation with the added amount of dissolved sulfur for a concentration range between 500 ppm and 10 000 ppm (Fig. 12). Below 500 ppm, the total-S signal was unchanged however (with a recorded intensity

Table 3. Core ER-CS04. Comparison between substratum analysis and surface analysis by WD-XRF

	SiO_2	Al_2O_3	Fe_2O_3	CaO	MgO	K_2O	TiO_2	S	MnO
	%	%	%	%	%	%	%	%	%
Substratum	43.87	21.46	8.16	1.07	2.19	1.76	0.78	1.60	0.05
Surface	44.63	21.53	8.00	1.07	2.17	1.79	0.80	1.79	0.05
Relative variation	*1.72*	*0.33*	*1.98*	*0.00*	*0.92*	*1.69*	*2.53*	*11.21*	*0.00*

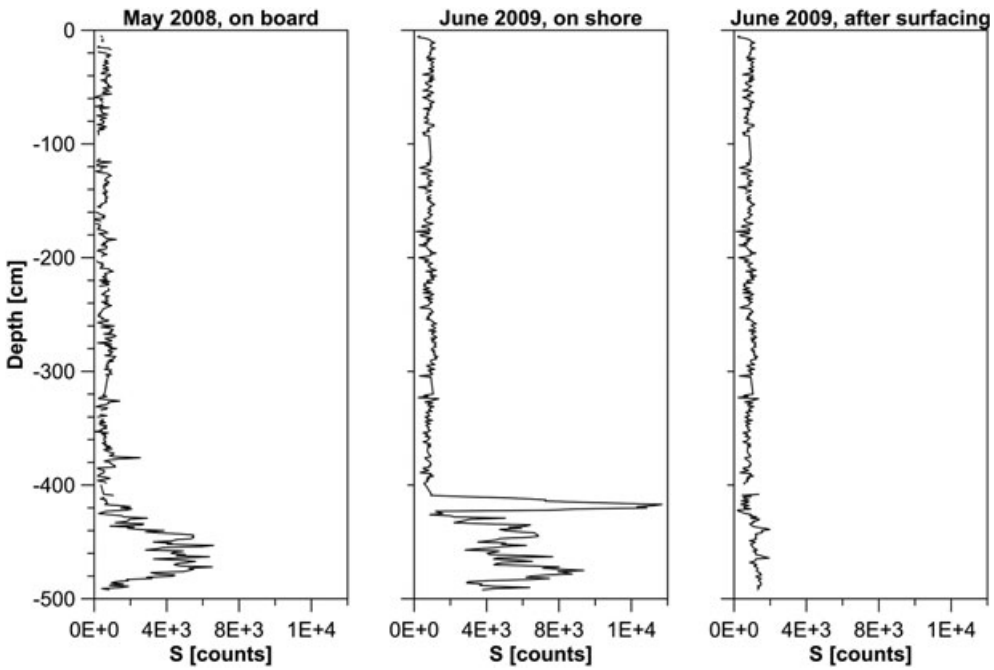

Figure 13. Core ER-CS04. High resolution total-S profile measured by XRF-CS at the surface of split core section *versus* depth in different condition: total-S measured onboard during the scientific cruise (left hand graph), total-S measured after one year without modification of the surface (middle graph) and total-S measured after one year and after a new surfacing (right hand graph).

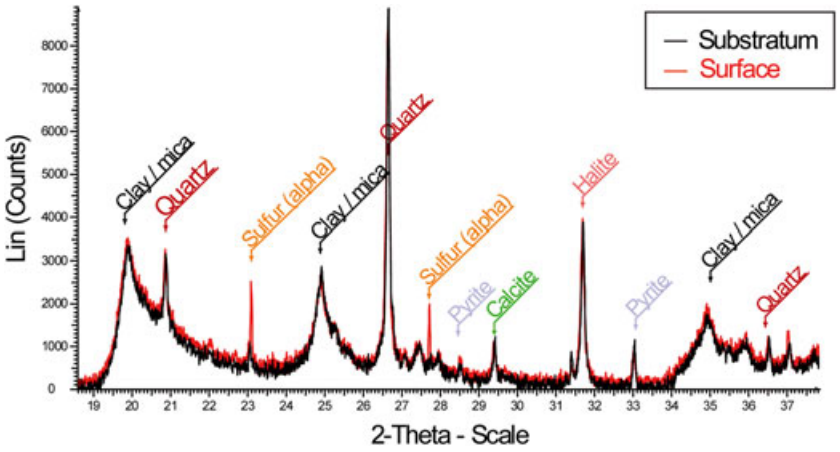

Figure 14. Core ER-CS04. Comparison between substratum (in black) analysis and surface (in red) analysis by XRD in section 6 (picture presented in Fig. 1).

about 2400cts for sulfur concentration of 0, 100 ppm and 200 ppm) probably because being lower than the DL. This 500-ppm threshold value is actually higher than the largest TDS content determined onboard by colorimetry on core ER-CS04 (i.e. maximum value of 225 ppm). Therefore, our series of experiments described above suggest that dissolved sulfur related to pore water or seawater cannot contribute significantly to the XRF-CS total-S count rate signal obtained at the surface of split wet sediment core.

Finally, taking a step further, we investigated whether this total-S signal could be related to a surficial enrichment in solid sulfur. To this purpose, we compared total-S down core profiles for the same core section, but acquired at different times over a 1-year period: (1) first on board, soon after core recovery, (2) about one year after recovery, in the onshore laboratory without any additional preparation of the surface sediment, and (3) one year later, but after re-surfacing the core section (Fig. 13). The initial total-S profile acquired on board displays a relatively flat pattern from the core top to about 400-cm depth, with total-S values of 100–200cts, but then increases suddenly to around 6600cts. The same trend was also observed after one year, but without additional preparation of the surface sediment. The increase of the signal, near 400-cm depth, was even greater, reaching a maximum value of about 13 700cts. However, after resurfacing the sediment surface, we clearly observe the disappearance of this sulfur enrichment. Most likely, this finding suggests that the cause of sulfur enrichment at about 400-cm depth in core ER-CS04 was related to a localized enrichment at the surface of the core. To validate this result, the corresponding surficial sediment was carefully sampled and analyzed by WD-XRF and compared with the bulk sediment composition (Table 3). The results indicate that the abundances of all major elements do not vary by more than 2%, except for sulfur, which was 10% enriched in the surface sediment layer compared to bulk sediment values. An XRD analysis of the sample surface showed the appearance of α-sulfur at the surface of split core in section 6 (Fig. 14).

Taken together, the above consideration suggests that the initial enrichment in sulfur at the surface of the core section most likely resulted from the oxidation of a fraction of TDS from pore waters after core opening. It is possible that oxidation of dissolved sulfides at the surface of the core led to the formation of a thin layer of solid sulfate deposit. This sulfur enriched layer represents a very nice target for X-ray analysis with respect to the effective penetration depth (10–20 μm) at the low K line energy S. The solid surface film is also stable with time. It hence offers the opportunity to locate sediment horizons characterized by high dissolved sulfide contents in marine sediments, even months or years after coring.

Conclusions

In this study, we have investigated the utility of acquiring XRF-CS high-resolution profiles of sulfur along marine sediment cores. Our results show that the contribution of dissolved forms of sulfur from both seawater and pore waters has negligible influence on total-S XRF-CS count rates. The combination of total-S profiles by XRF-CS with sulfate-bearing S and total-S WD-XRF analyses and XRD quantitative determinations of pyrite abundance on selected discrete samples demonstrates that this technique has the potential for providing routine, rapid and high-resolution estimates of pyrite mineral distribution along marine sediment cores from oxygen-depleted settings, of course under the prerequisite condition that pyrite represents the dominant sulfur-bearing mineral phase in the sediment, in particular relative to sulfate minerals The presence of pronounced sulfur enrichment in XRF-CS profiles can also reflect the presence of surficial layer of solid sulfate related to the oxidation of pore water dissolved sulfides after core opening. This thin and stable surficial sulfate layer can be detected by XRF-CS a long time after the coring.

Acknowledgements

The authors are grateful to B. Dennielou, A. Roubi and M. Rovere for the sample provided, their technical support and for several stimulating discussions. Thanks to J.C. Caprais and P. Pignet of Laboratoire de Microbiologie des Environnements Extrêmes of Ifremer for this analysis on pore water.

References

[1] T.O. Richter, S. Van Der Gaast, B. Koster Aad Vaars, R. Gieles, H. C. De Stigter, H. De Haas and T.C.E. Van Weering. *The Avaatech XRF Core Scanner: Technical Description and Applications to NE Atlantic Sediments*. Geological Society, London, Special Publications, **2006**, *267*, 39–50.

[2] J.H.F Jansen, S.J Van der Gaast, B Koster, A.J Vaars, CORTEX, *a shipboard XRF-scanner for element analyses in split sediment cores*, Marine Geology, **1998** *151*, 143–153.

[3] I. W. Croudace, A. Rindby, R.G. Rothwell, *ITRAX: Description and Evaluation of a New Multi-Function*. Geological Society, London, Special Publications **2006**, *267*, 51–63.
[4] J. Thomson, I.W. Croudace, R.G. Rothwell, A geochemical application of the ITRAX scanner to a sediment core containing eastern Mediterranean sapropel units, Geological Society, London, Special Publications **2006**, *267*, 65–77.
[5] M. Ziegler, T. Jilbert, G. J. de Lange, L. J. Lourens, G.-J. Reichart, *Bromine Counts from XRF Scanning as an Estimate of the Marine Organic Carbon Content of Sediment Cores*, Geochemistry, Geophysics, Geosystems, **2008**, pp. 9.
[6] R.G. Rothwell, B.A.A. Hoogakker, J.Thomson, I.W. Croudace, Turbidite emplacement on the southern Balearic Abyssal Plain (Western Mediterranean Sea) during Marine Isotope Stage 1–3: application of ITRAX XRF scanning of sediment cores to lithostratigraphic analysis, Geological Society, London, Special Publications **2006**, *267*, 79–98.
[7] T. Sakamoto, K. Kuroki, T. Sugawara, K. Aoike, K. Iijima, S. Sugisaki, Non-destructive X-ray fluorescence core-imaging scanner, Scientific Drilling, **2006**, *2*, 37–39.
[8] H. D. Schulz, M. Zabel. Marine geochemistry. *Geol Mag* **2002**, *139*, 455.
[9] J. S. Kuwabara, A. V. Geen, D. C. McCorkle, M. Bernhard. Dissolved sulfide distributions in the water column and sediment pore waters. *Geochim Cosmochim Acta* **1999**, *63*, 2199–2209.
[10] J.M. Brooks, A.L. Anderson, R. Sassen, I.R. MacDonald, M.C. Kennicutt II, N.L. Guinasso Jr., N.L., **1994**. Hydrate occurrences in shallow subsurface cores from continental slope sediments. In *Ann N Y Acad Sci*, *1994*, 715, 381–391.
[11] N. Sultan, B. Marsset, S. Ker, T. Marsset, M. Voisset, A. M. Vernant, G. Bayon, E. Cauquil, J. Adamy, J. L. Colliat, D. Drapeau. Hydrate dissolution as a potential mechanism for pockmark formation in the Niger delta. *J Geophys Res* **2010**, *115*, B08101.
[12] G. Bayon, D. Birot, L. Ruffine, J.-C. Caprais, E. Ponzevera, C. Bollinger, J.-P. Donval, J.-L. Charlou, M. Voisset, S. Grimaud. Evidence for intense REE scavenging at cold seeps from the Niger Delta margin. *Earth Planet Sci Lett* **2011**, *312*, 443–452.
[13] L. Ruffine, J. C. Caprais, G. Bayon, V. Riboulot, J. P. Donval, J. Etoubleau, D. Birot, P. Pignet, E. Rongemaille, B. Chazallon, S. Grimaud, J. Adamy, J. L. Charlou, M. Voisset. Investigation on the geochemical dynamics of a hydrate-bearing pockmark in the Niger Delta. *Mar Pet Geo* **2013**, *43*, 297–309.
[14] E. Suess. Marine cold seeps and their manifestations: geological control, biogeochemical criteria and environmental conditions. *Int J Earth Sci* **2014**, *103*(7), 1889–1916.
[15] A. Boetius, F. Wenzhöfer. Seafloor oxygen consumption fuelled by methane from cold seeps. *Nat Geosci* **2013**, *6*, 725–734.
[16] Y. C. Lim, S. Lin, T. F. Yang, Y. G. Chen, C. S. Liu. Variations of methane induced pyrite formation in the accretionary wedge sediments offshore southwestern Taiwan. *Mar Pet Geol* **2011**, *28*, 1829–1837.
[17] A. Peketi, A. Mazumdar, R. K. Joshi, D. J. Patil, P. L. Srinivas, A. M. Dayal. Tracing the Paleo sulfate-methane transition zones and H2S seepage events in marine sediments: an application of C–S–Mo systematics. *Geochem Geophys Geosyst* **2012**, *13*, 11.
[18] D. F. Chen, D. Feng, Z. Su, Z. G. Song, G. Q. Chen, L. M. Cathles. Pyrite crystallization in seep carbonates at gas vent and hydrate site. *Mater Sci Eng* **2006**, *26*, 602–605.
[19] G. J. Weltje, R. Tjallingii. Calibration of XRF core scanners for quantitative geochemical logging of sediment cores: theory and application. *Earth Planet Sci Lett* **2008**, *274*, 423–438.
[20] M. Pelikànovà. Determination of sulphur in silicate and carbonate rocks by wavelength dispersive XRF. *Fresenius Z Anal Chem* **1985**, *320*, 338–340.
[21] R. Jenkins, *Practical X-Ray Spectrometry*, book (1st edn **1967**), 93–94.
[22] G. J. Weltje et al., Prediction of geochemical composition from XRF core scanner data: a new multivariate approach including automatic selection of calibration samples and quantification of uncertainties, DPER volume: (Eds: I. W. Croudace, R. G. Rothwell), *Micro-XRF Studies of Sediment Cores, Developments in Paleoenvironmental Research 17*, **2015**.
[23] M. Bloemsma, Semi-automatic core characterisation based on geochemical logging data, Msc thesis Geomatics, **2010**.
[24] T. Monecke, S. Köhler, R. Kleeberg, P. Herzig, J. B. Gemmell. Quantitative phase-analysis by the rietveld method using X-ray powder-diffraction data: application to the study of alteration halos associated with volcanic-rock-hosted massive sulfide deposits. *Canad Min* **2001**, *39*, 1617–1633.
[25] M. Loubser, S. Verryn. Combining XRF and XRD analyses and sample preparation to solve mineralogical problems. *Geo Soc South Africa* **2008**, *111*, 229–238.
[26] L. B. McCusker, R. B. Von Dreele, D. E. Cox, D. Louër, P. Scardie. Rietveld refinement guidelines. *J Applied Crystallography* **1999**, *32*, 36–50.
[27] R. Tjallingii, U. Röhl, M. Kölling, T. Bickert. Influence of the water content on X-Ray fluorescence core-scanning measurements in soft marine sediments. *Geochem Geophys Geosyst* **2007**, 8.
[28] M. Zabel, R. R. Schneider, T. Wagner, A. T. Adegbie, U. de Vries, S. Kolonic. Late Quaternary climate changes in Central Africa as inferred from terrigenous input to the Niger Fan. *Quatern Res* **2001**, *56*(2), 207–217.